ACS Catalysis

pubs.acs.org/acscatalysis
Research Article

Regio- and Stereoselective Lactone Polymerization: Divergent Effect of Catalyst Modification and Monomer Structure

Yolanda Rusconi, Massimo C. D'Alterio, Sarah M. Severson, Claudio De Rosa, Geoffrey W. Coates,* and Giovanni Talarico*

Cite This: *ACS Catal.* 2026, 16, 9397−9405
Read Online

ACCESS | Metrics & More | Article Recommendations | Supporting Information

ABSTRACT: Selective ring-opening polymerization (ROP) of chiral lactones enables access to biodegradable polyesters with precisely controlled microstructures. Here, combined DFT modeling and experimental validation elucidate how fine-tuning of enantiopure SalBinam aluminum catalysts (through introduction of bromine atoms and *tert*-butyl groups, respectively, in *ortho*- and *para*-positions) modulates regio- and stereocontrol in the ROP of methyl glycolide (MeG) and lactide (LA). Computations reveal that regioselectivity in MeG polymerization arises mainly from steric repulsion, with a small contribution from weak stabilizing C-H···Br interactions that favor ring-opening at the glycolic site, consistent with the experimentally enhanced regioselectivity for (*R*)-MeG. In contrast, the same steric congestion at the ligand's *ortho* positions destabilizes the key transition states in *rac*-LA polymerization, reducing the calculated stereoselectivity. Experiments confirm the predicted loss of stereocontrol, yielding nearly atactic PLA under standard conditions. Extension of the computational framework to *rac*-MeG polymerization promoted by racemic catalyst identified a low-barrier, stepwise *polymer chain exchange* pathway that rationalizes the experimentally observed syndiotacticity of poly(lactic-*co*-glycolic acid).

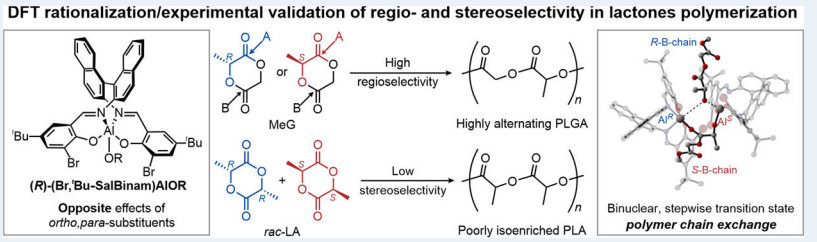

KEYWORDS: *ring-opening polymerization, DFT calculations, methyl glycolide, lactide, biodegradable polymers*

INTRODUCTION

Stereo- and regioselective ring-opening polymerization (ROP) of chiral lactones, such as lactide (LA) and 3-methyl glycolide (MeG), has emerged as a powerful synthetic strategy for producing aliphatic polyesters with precisely controlled microstructures.[1,2] These materials, derived from renewable feedstocks and characterized by biocompatibility and in vivo or industrial biodegradability, continue to attract growing interest for applications across biomedical engineering, drug delivery, and food packaging.[3−5]

Microstructure stereoregularity is highly desired to improve the material properties, such as crystallinity, mechanical strength, thermal behavior, or degradation kinetics. For instance, iso- and syndiotactic poly(lactic acid) (*i*- and *s*-PLA) are semicrystalline materials, with enhanced mechanical performance and improved thermal properties compared to atactic PLA, which is amorphous and mechanically softer.[6] Similarly, the microstructure of poly(lactic-*co*-glycolic acid) dramatically influences its hydrolytic stability: only alternating PLGA (*alt*-PLGA) displays a linear hydrolytic degradation behavior, derived from the presence of uniform lactic-glycolic acid linkages, which makes it suitable for drug delivery applications.[7−9] Additionally, stereoregular polyesters, such as *i*-PLA and *alt*-PLGA, have been proven to form stereocomplexes, an association of two polymer chains with opposite tacticity, expanding their use as high-performance materials.[10−12]

Pioneering work by Spassky et al. introduced an enantiopure (SalBinam)Al complex (**L1**^{R}AlOMe, Scheme 1A) that preferentially polymerized (*R*,*R*)-LA over (*S*,*S*)-LA by a $k_{R,R}$:$k_{S,S}$ of 20:1.[13] Replacement of the methoxy initiator with an isopropoxide (**L1**^{R}AlO^{i}Pr) enabled Ovitt et al. to achieve highly syndiotactic *s*-PLA (P_m = 0.96) from *meso*-LA (Scheme 1B).[14] Motivated by the strong enantioselectivity of this catalyst, Coates and coworkers explored its performance in the ROP of (*S*)-MeG (Scheme 1C), revealing a high regioselectivity favoring attack at the glycolic acid site (site B) over the lactic acid site (site A). Notably, a mismatch between the monomer and catalyst chirality resulted in higher regioselectivity (98% for **L1**^{R}AlO^{i}Pr) than the matched combination (78% for **L1**^{S}AlO^{i}Pr).[15] Catalyst optimization through the introduction of bromine atoms and *tert*-butyl groups, respectively, at the *ortho*- and *para*-positions of the phenol rings (**L2**AlO^{i}Pr) increased the regioselectivity of **L2**^{S}AlO^{i}Pr from 78% to 92%, leaving one of **L2**^{R}AlO^{i}Pr unchanged (Scheme 1D). The selective

Received: February 26, 2026
Revised: April 8, 2026
Accepted: April 10, 2026
Published: April 22, 2026

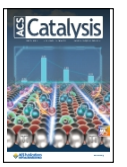

https://doi.org/10.1021/acscatal.6c01584
ACS Catal. 2026, 16, 9397−9405

enhancement of a single reaction pathway upon catalyst modification reveals aspects that cannot be readily rationalized with experimental observations alone.

To elucidate the origins of this phenomenon and to gain mechanistic insight into the roles of ligand substitution and monomer structure, we conducted a detailed computational analysis of the ROP promoted by **L2^{R}**AlO^{i}Pr with MeG and LA complemented by targeted experimental studies.[16]

Our investigation was also motivated by the reported activity of similar catalysts in the ROP of LA, such as racemic bimetallic (Sal-Binam)Al_2Me_4 complexes, bearing both *ortho*- and *para*-bromine or chlorine substituents, though exhibiting poor stereocontrol ($P_m = 0.57$[17] and $P_m = 0.50$[18]). The corresponding enantiopure *ortho-para*-Br complex, recently synthesized by Tong and coworkers, showed a ratio between the conversion of (*S*,*S*)-LA and (*R*,*R*)-LA of 1.39 in the respective ROPs, further confirming its low stereoselectivity.[19] Notably, bimetallic analogues lacking *ortho* substituents, with either iodide or methyl groups in *para* position, remained highly stereoselective toward *rac*-LA ($P_m = 0.92$ and $P_m = 0.93$ in the presence of BnOH),[19] highlighting how the observed decrease in stereoselectivity arises from steric congestion at the *ortho* positions rather than from any intrinsic mono- versus bimetallic effect.

We recently built a computational model based on density functional theory (DFT) calculations to explain the stereoselectivity of the prototype **L1^{R}**AlOMe system in the ROP of *rac*-LA.[20] In this model, the catalyst active species is hypothesized to adopt a fluxional octahedral geometry during the polymerization, displaying several configurations along the pathway (Scheme S1). Depending on how the [ONNO] ligand is wrapped around the metal, a *fac-fac* (*ff*) or *fac-mer* (*fm*) isomer can form, which are easily interconverting. The asymmetric *fm* isomer can undergo an additional distinction between *fm*1 and *fm*2, depending on the coordinating positions of the monomer and initiator/polymer chain (Scheme S2). These features were found to be essential in rationalizing the stereocontrol of **L1^{R}**AlO^{i}Pr in the ROP of *rac*- and *meso*-LA, as well as its regiocontrol toward (*S*)- and (*R*)-MeG.[21,22] The computational background developed around these reactions motivated us to (1) understand the reasons why this specific catalyst modification (**L2^{R}**AlO^{i}Pr) dictates a higher regioselectivity toward (*R*)-MeG; (2) theoretically predict and experimentally prove the opposite behavior in the ROP of *rac*-LA (Scheme 1E); and (3) provide novel insights on the *polymer chain exchange mechanism* proposed in the literature but never verified theoretically.

COMPUTATIONAL DETAILS

All density functional theory calculations were performed using the Gaussian 16 package,[23] choosing B3LYP[24,25] functional for both optimization and energy refinement steps. In the optimization, a mixed basis set was used: 6-311G(d,p)[26,27] for Al, Def2SVP[28] for C, H, N, and O, and SDD[29] (with associated pseudopotential) for Br. In single-point calculations, dispersion effects have been modeled through D3BJ[30] empirical dispersion by Grimme; the 6-311G(d,p) basis set was used for Al, C, H, N and O atoms and the SDD basis set was used for Br. Solvent effects have been evaluated with the CPCM[31] solvation model and considering dichloromethane or toluene as solvents. M06 and ωB97XD functionals were also employed in single-point calculations to confirm the selectivity (see Table S1). Gibbs energy of the dinuclear species underwent correction of the translational entropies following the Martin correction,[32−35] adapted for DCM. Noncovalent interaction (NCI) analysis was performed using the NCIPLOT4[36] software. VMD software[37] was used to visualize the generated isosurfaces. NCI quantification has been obtained with Atoms in Molecules (AIM) topological analysis[38] using the Multiwfn program.[39] The buried volume (%V_{Bur}) analysis was performed with the SambVca 2.1 tool.[40] Additional computational details are available in the Supporting Information.

Scheme 1. Ring-Opening Polymerizations of *rac*-LA Promoted by L1^{R}AlOMe, *meso*-LA, and (*S*)-MeG Promoted by L1^{R}AlO^{i}Pr (Previous Work, A−C) and ROPs of (*S*)-MeG and *rac*-LA Promoted by L2^{R}AlO^{i}Pr (This Work, D and E).

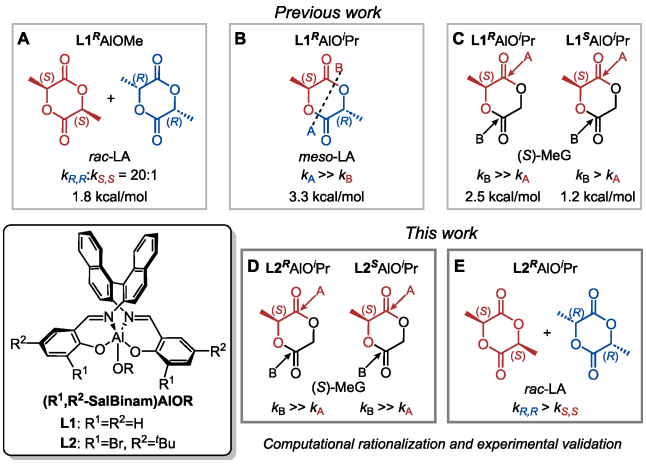

RESULTS AND DISCUSSION

ROP proceeds through a coordination-insertion mechanism (Scheme S3), in which the two key transition states (TSs) are nucleophilic attack of the initiator on the monomer (TS1) and ring-opening of the monomer (TS2). The regiochemistry of the polymerization has been rationalized considering (1) chirality/wrapping mode of the catalyst (*ff*, *fm*1, and *fm*2), (2) stereo- and regio-chemistry of the propagating chain ((*S* or *R*)-A-chain and (*S* or *R*)-B-chain), and 3) monomer chirality/enantioface (*R*,*S*)/(*re*,*si*) (Scheme S4). Minimum energy paths (MEPs) are the result of a thorough conformational analysis carried out by combining two previously explored domains. The conformational analysis of the growing chain is reported in Scheme S5 and Figures S1−S3. Concerning the catalyst, *ff*, *fm*1, and *fm*2 configurations were systematically combined with the various minima of the chain. Conformational sampling of all transition states is presented in Tables S2 and S3.

In our work on the ROP of (*R*)- and (*S*)-MeG promoted by enantiopure **L1^{R}**AlO^{i}Pr, regioselectivity was ascribed to the presence of stronger steric ligand-chain interactions in the rate-determining steps (RDSs) for attack at the more hindered site A. The Gibbs energy differences ($\Delta\Delta G^{\ddagger}_{regio}$) calculated for the propagation were, respectively, 2.5 and 1.2 kcal·mol^{-1} for (*S*)- and (*R*)-MeG in dichloromethane (DCM). In all cases, an exchange of the monomer and polymer chain position was observed going from TS1-*fm*1 to TS2-*fm*2. The only exception is represented by attack at site A of (*S*)-MeG, for which ring-opening also occurs in a *fm*1 geometry. Interestingly, we observed that the preferred *S* and *R* monomer propagation occur on opposite monomer enantiofaces (*si* and *re* enantiofaces, respectively). This unusual

https://doi.org/10.1021/acscatal.6c01584
ACS Catal. 2026, 16, 9397−9405

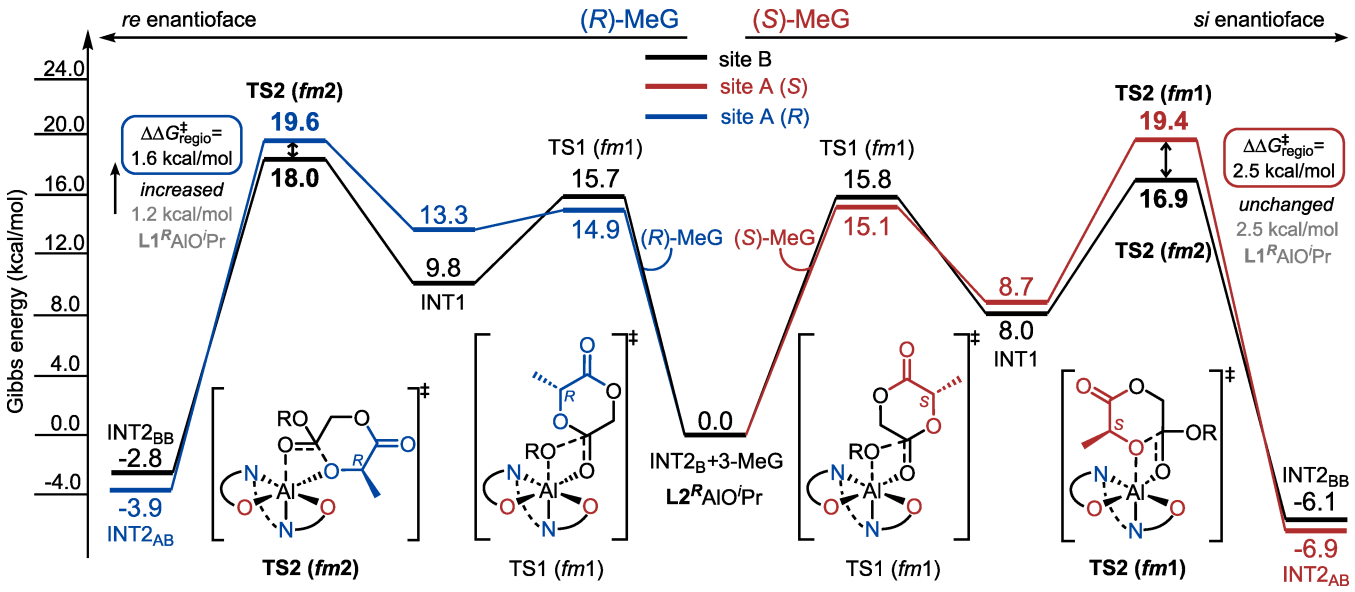

Figure 1. Minimum energy path for the propagation of the ring-opening polymerization of (*S*)- (right) and (*R*)-MeG (left) promoted by **L2**^{R}AlO^{i}Pr on a previously inserted B-chain. Attack at site B is reported in black, attack at site A of (*S*)-MeG in red and of (*R*)-MeG in blue.

behavior is attributed to the placement of the methyl group of the monomer as far as possible from the ligand framework to minimize steric repulsion.

Having carried out a detailed computational analysis on **L1**^{R}AlO^{i}Pr, we were intrigued by the observation that the **L2**^{R}AlO^{i}Pr catalytic system significantly increased regioselectivity toward (*R*)-MeG. We sought to apply our robust model to rationalize this system's regioselectivity, focusing on the propagation step, where the presence of the growing polymer chain becomes relevant. The main DFT findings are summarized in the minimum energy path reported in Figure 1. Gibbs energies are calculated with respect to the intermediates bearing the *S*- and *R*-B-chains + monomer ($INT2_B$ + MeG) at infinite distance. In all four cases, attack at site A or B of (*S*)- and (*R*)-MeG on a B-chain (favored in the first insertion), the ring-opening of the monomer (TS2) represents the RDS. As previously observed, opposite *re* and *si* enantiofaces are preferred, respectively, for (*R*)- and (*S*)-MeG, and a change from *fm*1 to *fm*2 occurs between TS1 and TS2, except for attack at site A of (*S*)-MeG. For this pathway, the calculated regioselectivity is 2.5 kcal·mol^{-1}, matching the $\Delta\Delta G^{\ddagger}_{regio}$ determined for **L1**^{R}AlO^{i}Pr. This result agrees with and explains the experimental observation that the *ortho*-Br modification of the **L2**^{R}AlO^{i}Pr catalyst does not enhance regioselectivity for (*S*)-MeG. Analysis of the optimized TS structures governing regioselectivity revealed that the *para*-^{t}Bu substituents only play a marginal role (consistently across all TSs) due to their distance from the catalytic pocket where the reaction takes place. The *ortho*-bromine atoms introduce additional unfavorable monomer/chain−ligand interactions; however, these are present in both geometries, dictating the regiochemistry. In fact, the preferred structures for site B (TS2-*fm*2-*si* in Figure 2A) and for site A (TS2-*fm*1-*si* in Figure 2B) are destabilized similarly, without changing the energy difference between them.

We further hypothesized that the halogen atoms could not only increase steric hindrance in specific conformations but also engage in hydrogen-bond-like noncovalent interactions with hydrogen atoms of the monomer or the growing chain. Weak stabilizing interactions between the ligand framework and monomer or

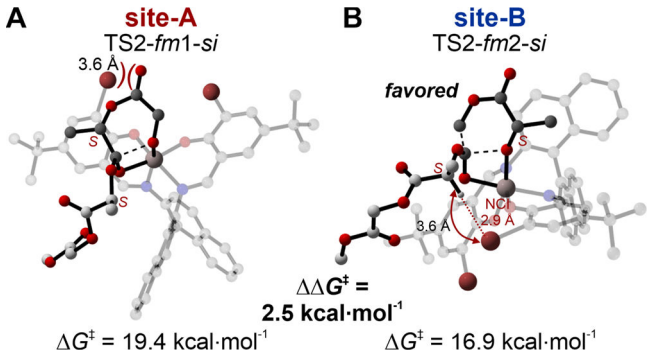

Figure 2. DFT geometries of the RDSs for attack at site A (A) and B (B) promoted by **L2**^{R}AlO^{i}Pr on a previously inserted B-chain of (*S*)-MeG. Carbon atoms of the inserting monomer are represented in dark gray, while those of the growing chain in white. H atoms are omitted for clarity.

growing chain are increasingly being explored as possible factors affecting the stereo- or regioselective outcomes in polymerization catalysis.[41−43] This hypothesis was tested through NCI analysis,[36,37] which represents NCIs as isosurfaces between interacting atoms: strong attractive interactions appear in blue, weak stabilizing ones in green, and repulsive interactions in red. In TS2-*fm*1-*si* for attack at site A, the *fm*1 configuration determines that no hydrogens are positioned near the bromine atoms to allow such interactions.

However, in the corresponding TS2-*fm*2-*si* structure for attack at the favored site B, a hydrogen of a methine group of the growing chain lies 2.9 Å from one of the Br atoms. As indicated by the green NCI isosurface (Figure S4), a weak stabilizing interaction is indeed present.

While catalyst modification moving from **L1**^{R}AlO^{i}Pr to **L2**^{R}AlO^{i}Pr does not improve regioselectivity toward (*S*)-MeG, a substantial effect has been calculated for (*R*)-MeG ($\Delta\Delta G^{\ddagger}_{regio}$ = 1.6 kcal·mol^{-1}, Table 1). In fact, this value is higher than the one previously calculated for **L1**^{R}AlO^{i}Pr[22] and is consistent with the experimentally observed enhancement of regioselectivity when **L2**^{R}AlO^{i}Pr is used (from 78 to 92%).[16]

https://doi.org/10.1021/acscatal.6c01584
ACS Catal. 2026, 16, 9397−9405

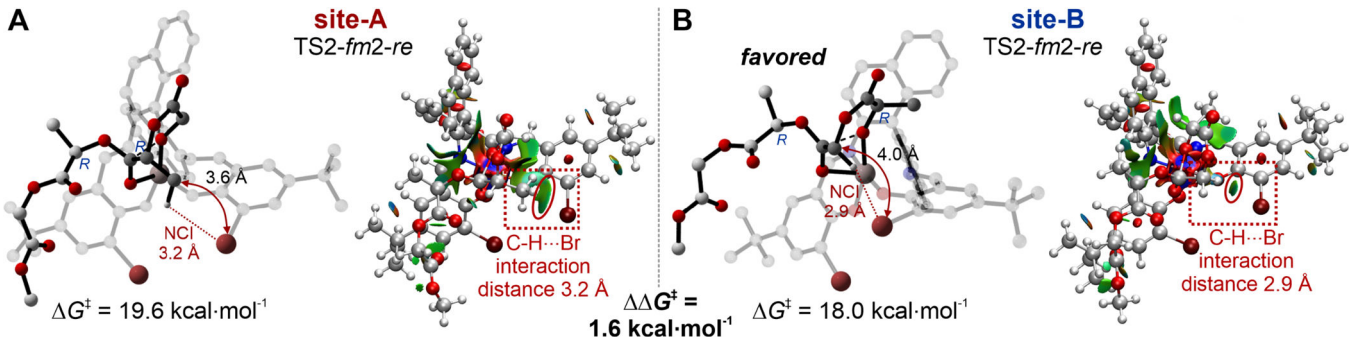

Figure 3. DFT geometries and NCI analyses of the RDSs for attack at sites A (A) and B (B) promoted by **L2^{R}**AlO^{i}Pr on a previously inserted B-chain of (*R*)-MeG. Carbon atoms of the inserting monomer are represented in dark gray, while those of the growing chain in white in the optimized geometries.

Inspection of the optimized TS structures of the RDS revealed an unfavorable steric clash between the methyl group of the monomer undergoing attack at site A positioned at 3.6 Å from one Br atom, which increases the energy of this TS (Figure 3A, left). No such steric interaction is present for attack at site B because the orientation of the monomer keeps the methyl group away from the bromine atoms, thereby avoiding additional steric repulsion (Figure 3B, left).

The NCI analysis for (*R*)-MeG shows green isosurfaces for both structures; the interaction between a Br atom and a hydrogen of the methyl group is established at a distance of 3.2 Å for site A (Figure 3A, right). In contrast, the TS2 structure arising from attack at site B is stabilized by a C-H···Br interaction involving a methylene hydrogen (Figure 3B, right). This interaction is stronger than that observed for site A because (1) the C-H···Br distance is shorter (2.9 Å vs. 3.2 Å) and (2) the interacting hydrogen belongs to a methylene group, and it bears a stronger partial positive charge due to electronic delocalization effects being in alpha position to a carbonyl carbon. The stronger interaction in the site-B TS was also confirmed by AIM topological analysis (Figure S5).[38] However, we argue that the main factor responsible for the high regioselectivity has steric roots.[44] Indeed, the %V_{Bur} analysis[40] revealed higher occupancy of the north-west (NW) quadrant of the catalytic pocket of **L2^{R}**AlO^{i}Pr, where Br atoms are located, compared to **L1^{R}**AlO^{i}Pr (54.0% *vs* 60.6%, Figure 4), while the other occupancies remained basically unchanged.

Table 1. DFT Gibbs Energies ($\Delta G^{\ddagger}$ in kcal·mol^{-1}) of the Minimum-Energy TSs for the ROP of (*S*)- and (*R*)-MeG Promoted by L2^{R}AlO^{i}Pr and ROP of (*R*,*R*)- and (*S*,*S*)-LA Promoted by L1^{R}AlO^{i}Pr and L2^{R}AlO^{i}Pr[a]

monomer	wrapping mode TS1-TS2[b]	TS1[c]	TS2[c]
L2^{R}AlO^{i}Pr			
(*S*)-MeG, A	*fm*1-*fm*1 (*si*)	15.1	**19.4**
(*S*)-MeG, B	*fm*1-*fm*2 (*si*)	15.8	**16.9**
(*R*)-MeG, A	*fm*1-*fm*2 (*re*)	14.9	**19.6**
(*R*)-MeG, B	*fm*1-*fm*2 (*re*)	15.7	**18.0**
L1^{R}AlO^{i}Pr[20]			
(*R*,*R*)-LA	*fm*1-*fm*2 (*re*)	12.7	**14.4**
(*S*,*S*)-LA	*ff*-*ff* (*re*)	**16.2**	12.1
L2^{R}AlO^{i}Pr			
(*R*,*R*)-LA	*fm*1-*fm*2 (*re*)	15.7	**18.0**
(*S*,*S*)-LA	*ff*-*ff* (*re*)	**18.7**	14.6

[a]The RDSs are reported in bold. [b]Enantiofaces are reported in parentheses. [c]$\Delta G^{\ddagger}$s reported in kcal·mol^{-1}.

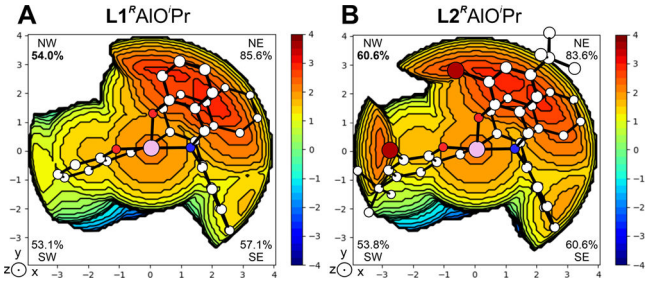

Figure 4. Steric maps obtained *via* %V_{Bur} analysis of the octahedral catalytic pockets of **L1^{R}**AlO^{i}Pr (A) and **L2^{R}**AlO^{i}Pr (B), highlighting the higher steric hindrance of the NW quadrant where *ortho*-Br atoms are present.

Replacement of the Br and ^{t}Bu substituents with methyl groups allowed a quantification of the purely steric contribution. The regioselectivity decreases from 1.6 to 1.3 kcal·mol^{-1}, confirming that the NCI contributes to selectivity but is clearly not the only factor involved. In summary, the unchanged regioselectivity of **L2^{R}**AlO^{i}Pr toward (*S*)-MeG arises from the presence of destabilizing interactions in both the RDSs, which preclude further energetic differentiation between the competing pathways.

In contrast, the enhanced selectivity observed for (*R*)-MeG originates primarily from steric destabilization of the site A TS by the *ortho* substituents, with secondary stabilization of the site B pathway arising from weak C-H···Br NCIs.

The not-straightforward impact of the Br-^{t}Bu substituents on MeG regioselectivity prompted us to investigate whether the same structural features could also affect the stereochemical outcome of *rac*-LA polymerization in toluene. In our previous study on the ROP of *rac*-LA promoted by **L1^{R}**AlO^{i}Pr, we calculated a stereoselectivity of 1.8 kcal·mol^{-1} during propagation, favoring insertion of (*R*,*R*)-LA.[20] This $\Delta\Delta G^{\ddagger}_{stereo}$ results from the difference in energy between the RDS formed by TS2-*fm*2-*re* for (*R*,*R*)-LA (14.4 kcal·mol^{-1}, Table 1) and TS1-*ff*-*re* for (*S*,*S*)-LA (16.2 kcal·mol^{-1}, Table 1), respectively. Comparison of these results with those obtained for MeG led to several conclusions for the ROP of *rac*-LA: (1) the *ff* configuration is relevant; (2) the *re* enantioface is preferred for both monomer enantiomers; and (3) either nucleophilic attack or ring-opening can be RDSs.

Notably, inspection of the TS2-*fm*2-*re* for (*R*,*R*)-LA geometry revealed that the incoming monomer is close to the *ortho*-position

https://doi.org/10.1021/acscatal.6c01584
ACS Catal. 2026, 16, 9397−9405

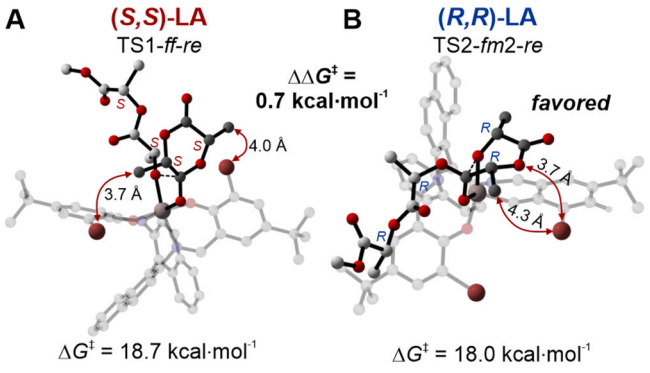

Figure 5. DFT geometries of the RDSs for (*S*,*S*)-LA (A) and (*R*,*R*)-LA (B) promoted by **L2**^{R}AlO^{i}Pr on a previously inserted (*S*,*S*)- or (*R*,*R*)-chain. Carbon atoms of the inserting monomer are represented in dark gray, while those of the growing chain in white. H atoms are omitted for clarity.

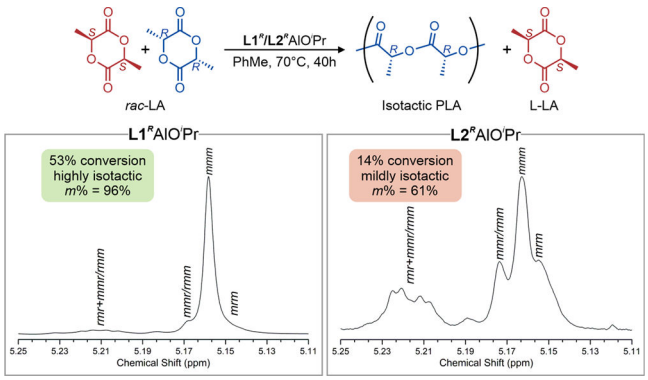

Figure 6. Methine region of the homonuclear-decoupled ^{1}H NMR spectrum of poly(lactic acid) prepared with **L1**^{R}AlO^{i}Pr (left) and **L2**^{R}AlO^{i}Pr (right).

of the ligand's phenoxide ring (Figure S6). This observation may suggest that increasing steric bulk at this position would *destabilize* this TS and consequently reduce the overall stereoselectivity. Such an effect would introduce an additional layer of complexity, as optimal catalyst tuning would become dependent on the monomer structure. We sought to verify this hypothesis by computationally optimizing the ROP of *rac*-LA initiated by **L2**^{R}AlO^{i}Pr, and we indeed calculated a decrease of stereoselectivity from 1.8 to 0.7 kcal·mol^{-1} (Table 1). The minimum energy path for both LA enantiomers, reported in Figure S7, involves the same configurations found for **L1**^{R}AlO^{i}Pr with higher activation energies. The enantioselectivity-determining steps are TS2-*fm*2-*re* for (*R*,*R*)-LA (18.0 kcal·mol^{-1}, Table 1) and TS1-*ff*-*re* for (*S*,*S*)-LA (18.7 kcal·mol^{-1}, Table 1). In the *ff* geometry, both Br atoms bump into the two methyl substituents of the monomer at distances of 3.7 and 4.0 Å (Figure 5A). In the *fm*2 TS, the monomer is deformed and points toward one Br atom, creating unfavorable interactions with the latter (distances of 3.7 and 4.3 Å, Figure 5B). These features result in an increase in the activation barriers (the catalyst is expected to be less active) and a decrease in the energy gap between these two structures and therefore a lower stereoselectivity. It is worth noting that the activation barriers for the ROP of LA are comparable to those of attack at the lactyl site of MeG (calculated in toluene and DCM, respectively).

To experimentally validate these computational predictions, we next evaluated the activity and stereochemical outcome of the ROP of *rac*-LA promoted by **L2**^{R}AlO^{i}Pr under standard lactide polymerization conditions (toluene, 70 °C). First, we reproduced the well-known ROP of *rac*-LA mediated by **L1**^{R}AlO^{i}Pr, ensuring that the polymerization was carried out under identical conditions to those described in the literature to provide a reliable reference point.[13] A 53% conversion was reached in 40 h. Investigation of the methine resonances in the homonuclear-decoupled ^{1}H NMR spectrum of the polymer (Figures S8 and S9 for stereoselectivity calculations) confirmed that the obtained polymer is isotactic with a *m*% (percentage of adjacent linkages with a *meso* configuration) of 96% (Figure 6, left). We then investigated the behavior of the modified catalyst **L2**^{R}AlO^{i}Pr under the same reaction conditions. The polymerization only reached 14% conversion in 40 h, and the calculated *m*% of the final polymer was 61% (Figure 6, right). The small conversion confirmed the lower activity of this catalytic system and the poor isotactic microstructure agreed with the decrease in stereoselectivity calculated computationally by us (0.7 kcal·mol^{-1}, Table 1).

Encouraged by the good agreement between theory and experiments, we extended our computational investigation to rationalize the polymerization behavior when a racemic mixture of chiral catalysts is used, instead of the enantiopure *R* catalyst discussed above. A syndiotactic-enriched microstructure is observed when *rac*-MeG is polymerized in the presence of racemic **L2**^{rac}AlO^{i}Pr. Previous kinetic resolution experiments reported by Lu et al. showed that, when used to polymerize *rac*-MeG, the *R* catalyst preferentially inserts the *S* over *R* monomer with a 3:1 ratio ($k_{rel} = 3$).[16]

This is reflected in the calculated 1.1 kcal·mol^{-1} difference between the RDSs for attack at site B of the two monomers reported above (16.9 kcal·mol^{-1} for (*S*)-MeG and 18.0 kcal·mol^{-1} for (*R*)-MeG, Figure 1 and Table 1).

When racemic **L2**^{rac}AlO^{i}Pr is employed, each catalyst enantiomer consumes its preferred monomer, generating two propagating intermediates with opposite chirality between the catalyst and growing chain: **L2**^{R}Al-*S*-chain and **L2**^{S}Al-*R*-chain, identified as "mismatch" intermediates (opposite chirality of the catalyst and growing chain) for analogue bipyrrolidine aluminum catalysts.[45] These species are less stable (−12.6 kcal·mol^{-1}, Figure S10) than their corresponding "match" intermediates **L2**^{R}Al-*R*-chain and **L2**^{S}Al-*S*-chain (−14.4 kcal·mol^{-1}, Figure S10), as also observed for Spiro-Salen Y systems for the ROP of β-butyrolactone.[46] Interconversion of these species can be achieved through a *polymer chain exchange* mechanism, hypothesized for these Al systems and subsequently extended to a variety of catalytic systems.[47−50]

In more detail, two mismatch propagating intermediates come closer together to form a dinuclear species in which each chain bridges the two Al centers with its alkoxo and carbonyl oxygen atoms (INT_{10cts} (*RS*-*SR*), 2.6 kcal·mol^{-1}, Figure 7). Then, chain transfer between the two catalytic systems can occur. First, we identified a straightforward four-center, bridging μ^{2}-alkoxo dinuclear TS (TS_{CT}-concerted, Figure 7) corresponding to a concerted exchange pathway, the most commonly hypothesized (though never reported) route.[46,51] In the latter, both polymer chains exchange at the same time, each binding only with its terminal oxygen to the aluminum atoms, therefore creating a tight catalytic pocket (Figure 8). This sterically encumbered structure exhibited an activation barrier of 24.7 kcal·mol^{-1}, (much) higher than the propagation steps reported in Table 1 (13.8 kcal·mol^{-1} after translational entropies correction), which made it not feasible. This high

https://doi.org/10.1021/acscatal.6c01584
ACS Catal. 2026, 16, 9397−9405

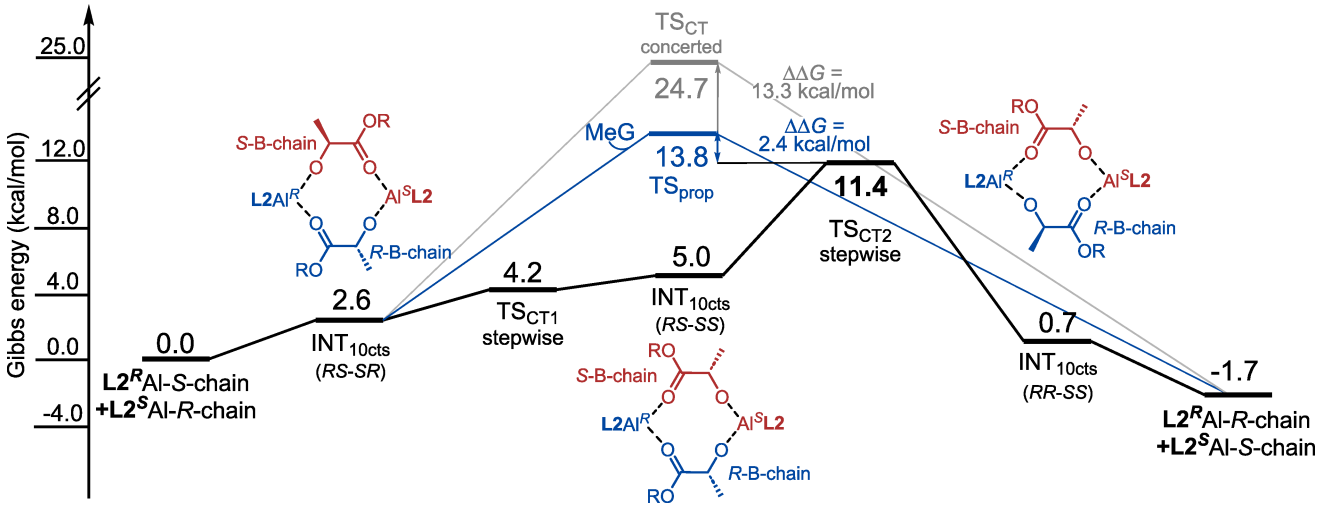

Figure 7. Minimum energy path of the polymer chain exchange mechanism promoted by **L2^R**AlO^{i}Pr. The Gibbs and activation energies of the TS for propagation are reported in blue while those of the TS$_{CT}$-concerted in light gray. All energies are obtained from the translational entropic correction.

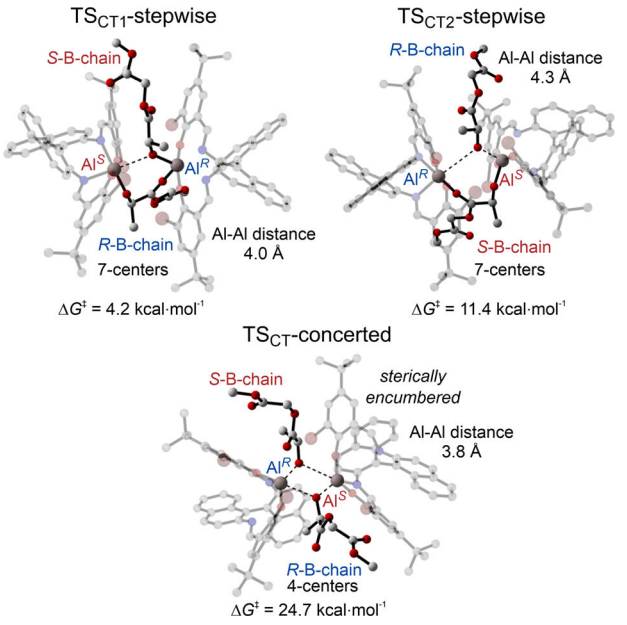

Figure 8. Comparison of the DFT-optimized geometries of the concerted (more congested, bottom) and stepwise (top) chain exchange TSs.

activation barrier might explain the lack of computational ROP mechanisms involving monomer propagation *and* polymer chain exchange in literature. We therefore investigated an alternative stepwise mechanism, consisting of two TSs, in which one polymer chain at a time acts as a μ^2-κ^2 ligand, simultaneously coordinating to both aluminum centers with two oxygen atoms, while the second chain migrates from one metal center to the other (TS$_{CT}$-stepwise, Figures 7 and 9). After the first chain transfer, a new 10-center intermediate is formed with one of the two chains switched (INT$_{10cts}$ (*RS-SS*), 5.0 kcal·mol^{-1}). At this point, the second chain can migrate (TS$_{CT2}$-stepwise). The two TSs involved in the stepwise mechanism create a wider catalytic pocket, characterized by a higher Al-Al distance (4.0-4.3 Å, Figure 8), and therefore much lower barriers, 4.2 and 11.4 kcal·mol^{-1}, below those calculated for the propagation.

Eventually, the 10-center species with switched chains is obtained (INT$_{10cts}$ (*RR-SS*), 0.7 kcal·mol^{-1}), and it dissociates to the match propagating intermediates (see Figure S11 for optimized structures of INT$_{10cts}$). All the above-reported values are the result of translational entropy correction.[32] For comparison between corrected and non-corrected values, see Table S4. These results suggest that polymer chain exchange is kinetically accessible, establishing a pre-equilibrium between match and mismatch intermediates, as summarized in Figure 9. Interestingly, the continuous reshuffling of chain ends through this low-barrier exchange mechanism places greater emphasis on the relative activation energies of the intermediates. Accordingly, the low syndiotacticity observed for **L2^{rac}**AlO^{i}Pr with *rac*-MeG can be rationalized by the mismatch intermediates exhibiting lower activation barriers, for which the energetic preference for syndiotactic placement is minimal (0.4 kcal·mol^{-1}, $P_{r\,(exp)}$= 0.71; Figure 9).

CONCLUSIONS

In summary, the combined computational and experimental investigation reported herein elucidates the origins of both regio- and stereoselectivity in the ROP of chiral lactones promoted by SalBinam aluminum complexes. Moreover, it demonstrates how subtle ligand modifications can profoundly influence catalytic behavior in a monomer-dependent manner that is difficult to anticipate without computational insight. Introduction of *ortho*-bromine and *para-tert*-butyl substituents in **L2^R**AlO^{i}Pr modulates the sterics of the active site, enhancing regioselectivity for ROP of (*R*)-MeG through a combination of steric repulsion and weak stabilizing C-H···Br interactions. In contrast, this catalyst tuning is ineffective for ROP of (*S*)-MeG and simultaneously diminishes stereocontrol in the ROP of *rac*-LA by destabilizing key enantioselectivity-determining transition states. The excellent agreement between theory and experiments validates the mechanistic relevance of our DFT model, which highlights the role of ligand wrapping modes, active-site reorganization, and noncovalent interactions in governing selectivity. This framework was further extended, for the first time, to racemic mixtures of enantiopure catalysts. The newly identified low-energy, stepwise chain exchange pathway rationalizes the experimentally observed poor syndiotacticity of

https://doi.org/10.1021/acscatal.6c01584
ACS Catal. 2026, 16, 9397−9405

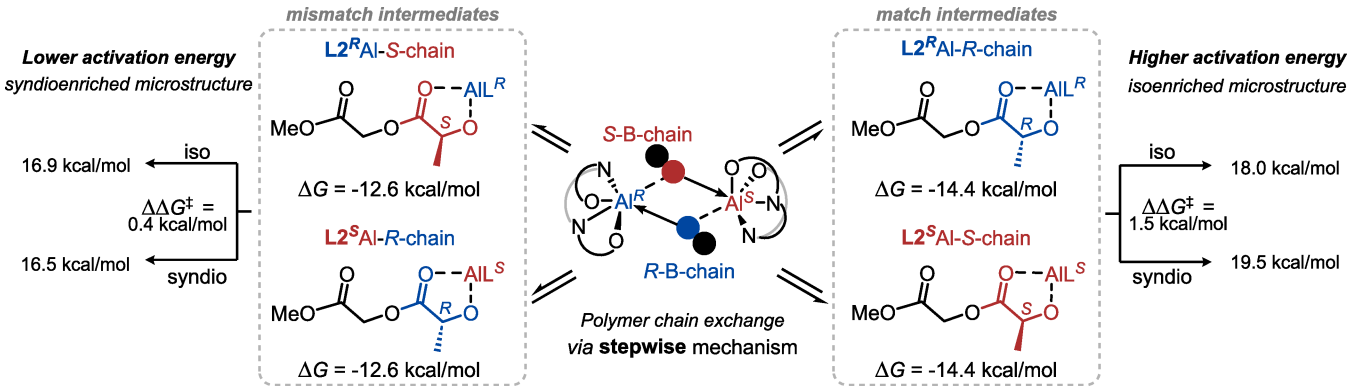

Figure 9. Gibbs energies (ΔG in kcal·mol^{-1}) for intermediates and transition states involved in the polymer chain exchange mechanism depending on the chirality of the catalyst and growing chain.

PLGA obtained with **L2**^{rac}AlO^{i}Pr. We are confident that these findings provide insights into how targeted ligand design can be used to tune and predict the performance of stereoselective ROP catalysts,[52] offering guiding principles for the development of new systems capable of producing biodegradable polyesters.

■ ASSOCIATED CONTENT

Supporting Information

The Supporting Information is available free of charge at https://pubs.acs.org/doi/10.1021/acscatal.6c01584.

Computational details, Schemes S1−S5, Figures S1−S13, and Tables S1−S4 (PDF)

Optimized Cartesian coordinates (XYZ)

■ AUTHOR INFORMATION

Corresponding Authors

Geoffrey W. Coates − *Department of Chemistry and Chemical Biology, Baker Laboratory, Cornell University, Ithaca, New York 14853-1301, United States;* orcid.org/0000-0002-3400-2552; Email: coates@cornell.edu

Giovanni Talarico − *Scuola Superiore Meridionale, Largo San Marcellino, 80138 Naples, Italy; Department of Chemical Sciences, University of Naples Federico II, Via Cintia, 80126 Naples, Italy;* orcid.org/0000-0002-4861-0444; Email: talarico@unina.it

Authors

Yolanda Rusconi − *Scuola Superiore Meridionale, Largo San Marcellino, 80138 Naples, Italy; Department of Chemical Sciences, University of Naples Federico II, Via Cintia, 80126 Naples, Italy;* orcid.org/0009-0006-9443-8944

Massimo C. D'Alterio − *Department of Chemical Sciences, University of Naples Federico II, Via Cintia, 80126 Naples, Italy;* orcid.org/0000-0003-0064-903X

Sarah M. Severson − *Department of Chemistry and Chemical Biology, Baker Laboratory, Cornell University, Ithaca, New York 14853-1301, United States;* orcid.org/0000-0001-9305-6270

Claudio De Rosa − *Department of Chemical Sciences, University of Naples Federico II, Via Cintia, 80126 Naples, Italy;* orcid.org/0000-0002-5375-7475

Complete contact information is available at: https://pubs.acs.org/doi/10.1021/acscatal.6c01584

Author Contributions

All authors have given approval to the final version of the manuscript.

Funding

This study was carried out within the MICS (Made in Italy—Circular and Sustainable) Extended Partnership funded from the European Union Next-Generation EU (Piano Nazionale di Ripresa e Resilienza (PNRR)—Missione 4 Componente 2, Investimento 1.3—D.D. 1551.11-10-2022, PE00000004).

Notes

The authors declare no competing financial interest.

■ ACKNOWLEDGMENTS

Y.R. thanks the U.S. Department of Energy (No. DE-FG02-05ER15687) for financial support for her research stay at Cornell University. The support from the Italian Ministry of University and Research (PRIN 2022, CUP E53D23008360006) is gratefully acknowledged. The authors acknowledge Dr. Yiye Lu for providing the catalyst.

■ REFERENCES

(1) Xie, X.; Huo, Z.; Jang, E.; Tong, R. Recent advances in enantioselective ring-opening polymerization and copolymerization. *Commun. Chem.* **2023**, *6*, 202.

(2) Shi, C.; Quinn, E. C.; Diment, W. T.; Chen, E. Y. X. Recyclable and (Bio)degradable Polyesters in a Circular Plastics Economy. *Chem. Rev.* **2024**, *124*, 4393−4478.

(3) Pang, X.; Zhuang, X.; Tang, Z.; Chen, X. Polylactic acid (PLA): Research, development and industrialization. *Biotechnol. J.* **2010**, *5*, 1125−1136.

(4) Ulery, B. D.; Nair, L. S.; Laurencin, C. T. Biomedical applications of biodegradable polymers. *J. Polym. Sci., Part B: Polym. Phys.* **2011**, *49*, 832−864.

(5) Sinclair, R. G. The Case for Polylactic Acid as a Commodity Packaging Plastic. *J. Macromol. Sci. A* **1996**, *33*, 585−597.

(6) Pan, P.; Liang, Z.; Zhu, B.; Dong, T.; Inoue, Y. Blending Effects on Polymorphic Crystallization of Poly(L-lactide). *Macromolecules* **2009**, *42*, 3374−3380.

(7) Pardeshi, S. R.; Nikam, A.; Chandak, P.; Mandale, V.; Naik, J. B.; Giram, P. S. Recent advances in PLGA based nanocarriers for drug delivery system: a state of the art review. *Int. J. Polym. Mater. Polym. Biomater.* **2023**, *72*, 49–78.
(8) Washington, M. A.; Swiner, D. J.; Bell, K. R.; Fedorchak, M. V.; Little, S. R.; Meyer, T. Y. The impact of monomer sequence and stereochemistry on the swelling and erosion of biodegradable poly(lactic-*co*-glycolic acid) matrices. *Biomaterials* **2017**, *117*, 66–76.
(9) Li, J.; Rothstein, S. N.; Little, S. R.; Edenborn, H. M.; Meyer, T. Y. The Effect of Monomer Order on the Hydrolysis of Biodegradable Poly(lactic-*co*-glycolic acid) Repeating Sequence Copolymers. *J. Am. Chem. Soc.* **2012**, *134*, 16352–16359.
(10) Huang, Y.-T.; Huang, H.-Y.; Cheng, J.-L.; Xie, M.; Feng, L.-W.; Cai, Z.; Zhu, J.-B. A Regio- and Stereoselective Ring-Opening Polymerization Approach to Isotactic Alternating Poly(lactic-*co*-glycolic acid) with Stereocomplexation. *Angew. Chem., Int. Ed.* **2025**, *64*, No. e202422147.
(11) Radano, C. P.; Baker, G. L.; Smith, M. R. Stereoselective Polymerization of a Racemic Monomer with a Racemic Catalyst: Direct Preparation of the Polylactic Acid Stereocomplex from Racemic Lactide. *J. Am. Chem. Soc.* **2000**, *122*, 1552–1553.
(12) Tsuji, H.; Yamasaki, M.; Arakawa, Y. Stereocomplex Formation between Enantiomeric Alternating Lactic Acid-Based Copolymers as a Versatile Method for the Preparation of High Performance Biobased Biodegradable Materials. *ACS Appl. Polym. Mater.* **2019**, *1*, 1476–1484.
(13) Spassky, N.; Wisniewski, M.; Pluta, C.; Le Borgne, A. Highly stereoelective polymerization of *rac*-(D,L)-lactide with a chiral Schiff's base/aluminium alkoxide initiator. *Macromol. Chem. Phys.* **1996**, *197*, 2627–2637.
(14) Ovitt, T. M.; Coates, G. W. Stereoselective Ring-Opening Polymerization of *meso*-Lactide: Synthesis of Syndiotactic Poly(lactic acid). *J. Am. Chem. Soc.* **1999**, *121*, 4072–4073.
(15) Lu, Y.; Swisher, J. H.; Meyer, T. Y.; Coates, G. W. Chirality-Directed Regioselectivity: An Approach for the Synthesis of Alternating Poly(Lactic-*co*-Glycolic Acid). *J. Am. Chem. Soc.* **2021**, *143*, 4119–4124.
(16) Lu, Y.; Coates, G. W. Pairing-Enhanced Regioselectivity: Synthesis of Alternating Poly(lactic-*co*-glycolic acid) from Racemic Methyl-Glycolide. *J. Am. Chem. Soc.* **2023**, *145*, 22425–22432.
(17) Santulli, F.; D'Auria, I.; Boggioni, L.; Losio, S.; Proverbio, M.; Costabile, C.; Mazzeo, M. Bimetallic Aluminum Complexes Bearing Binaphthyl-Based Iminophenolate Ligands as Catalysts for the Synthesis of Polyesters. *Organometallics* **2020**, *39*, 1213–1220.
(18) Wan, Y.; Bai, Y.; Xu, H.; He, J.; Zhang, Y. Highly Isoselective Ring-Opening Polymerization of *rac*-Lactide Using Chiral Binuclear Aluminum Catalyst. *Macromol. Rapid Commun.* **2021**, *42*, No. 2000491.
(19) Xie, X.; Huo, Z.; Crater, E. R.; Moore, R. B.; Tong, R. Enantioselective polymerization of racemic lactide for stereocomplex poly(lactic acid). *Chem. Catal.* **2025**, *5*, No. 101487.
(20) D'Alterio, M. C.; De Rosa, C.; Talarico, G. Stereoselective Lactide Polymerization: the Challenge of Chiral Catalyst Recognition. *ACS Catal.* **2020**, *10*, 2221–2225.
(21) D'Alterio, M. C.; De Rosa, C.; Talarico, G. Syndiotactic PLA from *meso*-LA polymerization at the Al-chiral complex: a probe of DFT mechanistic insights. *Chem. Commun.* **2021**, *57*, 1611–1614.
(22) Rusconi, Y.; D'Alterio, M. C.; De Rosa, C.; Lu, Y.; Severson, S. M.; Coates, G. W.; Talarico, G. Mechanism of Alternating Poly(lactic-*co*-glycolic acid) Formation by Polymerization of (*S*)- and (*R*)-3-Methyl Glycolide Using an Enantiopure Aluminum Complex. *ACS Catal.* **2024**, *14*, 318–323.
(23) Frisch, M. J.; Trucks, G. W.; Schlegel, H. B.; Scuseria, G. E.; Robb, M. A.; Cheeseman, J. R.; Scalmani, G.; Barone, V.; Petersson, G. A.; Nakatsuji, H.; Li, X.; Caricato, M.; Marenich, A. V.; Bloino, J.; Janesko, B. G.; Gomperts, R.; Mennucci, B.; Hratchian, H. P.; Ortiz, J. V.; Izmaylov, A. F.; Sonnenberg, J. L.; Williams; Ding, F.; Lipparini, F.; Egidi, F.; Goings, J.; Peng, B.; Petrone, A.; Henderson, T.; Ranasinghe, D.; Zakrzewski, V. G.; Gao, J.; Rega, N.; Zheng, G.; Liang, W.; Hada, M.; Ehara, M.; Toyota, K.; Fukuda, R.; Hasegawa, J.; Ishida, M.; Nakajima, T.; Honda, Y.; Kitao, O.; Nakai, H.; Vreven, T.; Throssell, K.; MontgomeryJr., J. A.; Peralta, J. E.; Ogliaro, F.; Bearpark, M. J.; Heyd, J. J.; Brothers, E. N.; Kudin, K. N.; Staroverov, V. N.; Keith, T. A.; Kobayashi, R.; Normand, J.; Raghavachari, K.; Rendell, A. P.; Burant, J. C.; Iyengar, S. S.; Tomasi, J.; Cossi, M.; Millam, J. M.; Klene, M.; Adamo, C.; Cammi, R.; Ochterski, J. W.; Martin, R. L.; Morokuma, K.; Farkas, O.; Foresman, J. B.; Fox, D. J. *Gaussian 16 Rev. C.01*, Gaussian Inc.: Wallingford, CT, **2016**.
(24) Lee, C.; Yang, W.; Parr, R. G. Development of the Colle-Salvetti correlation-energy formula into a functional of the electron density. *Phys. Rev. B* **1988**, *37*, 785–789.
(25) Becke, A. D. Density-functional exchange-energy approximation with correct asymptotic behavior. *Phys. Rev. A* **1988**, *38*, 3098–3100.
(26) McLean, A. D.; Chandler, G. S. Contracted Gaussian basis sets for molecular calculations. I. Second row atoms, Z=11–18. *J. Chem. Phys.* **1980**, *72*, 5639–5648.
(27) Binkley, S.; Pople, J. A.; Hehre, W. J. Self-Consistent Molecular Orbital Methods. 21. Small Split-Valence Basis Sets for First-Row Elements. *J. Am. Chem. Soc.* **1980**, *102*, 939.
(28) Weigend, F.; Ahlrichs, R. Balanced basis sets of split valence, triple zeta valence and quadruple zeta valence quality for H to Rn: Design and assessment of accuracy. *Phys. Chem. Chem. Phys.* **2005**, *7*, 3297–3305.
(29) Wadt, W. R.; Hay, P. J. Ab initio effective core potentials for molecular calculations. Potentials for main group elements sodium to bismuth. *J. Chem. Phys.* **1985**, *82*, 284–298.
(30) Grimme, S.; Antony, J.; Ehrlich, S.; Krieg, H. A consistent and accurate ab initio parametrization of density functional dispersion correction (DFT-D) for the 94 elements H-Pu. *J. Chem. Phys.* **2010**, *132*, 154104.
(31) Barone, V.; Cossi, M. Quantum Calculation of Molecular Energies and Energy Gradients in Solution by a Conductor Solvent Model. *J. Phys. Chem. A* **1998**, *102*, 1995–2001.
(32) Martin, R. L.; Hay, P. J.; Pratt, L. R. Hydrolysis of Ferric Ion in Water and Conformational Equilibrium. *J. Phys. Chem. A* **1998**, *102*, 3565–3573.
(33) Falivene, L.; Barone, V.; Talarico, G. Unraveling the role of entropy in tuning unimolecular vs. bimolecular reaction rates: The case of olefin polymerization catalyzed by transition metals. *Mol. Catal.* **2018**, *452*, 138–144.
(34) Besora, M.; Vidossich, P.; Lledós, A.; Ujaque, G.; Maseras, F. Calculation of Reaction Free Energies in Solution: A Comparison of Current Approaches. *J. Phys. Chem. A* **2018**, *122*, 1392–1399.
(35) Brotons Rufes, A.; Posada Pérez, S.; Poater, A. DFT in catalysis: Complex equations for practical computing applications in chemistry. *Digit. Chem. Eng.* **2026**, *18*, No. 100285.
(36) Boto, R. A.; Peccati, F.; Laplaza, R.; Quan, C.; Carbone, A.; Piquemal, J.-P.; Maday, Y.; Contreras-García, J. NCIPLOT4: Fast, Robust, and Quantitative Analysis of Noncovalent Interactions. *J. Chem. Theory Comput.* **2020**, *16*, 4150–4158.
(37) Humphrey, W.; Dalke, A.; Schulten, K. VMD Visual molecular dynamics. *J. Mol. Graph.* **1996**, *14*, 33–38.
(38) Bader, R. F. W. A quantum theory of molecular structure and its applications. *Chem. Rev.* **1991**, *91*, 893–928.
(39) Lu, T. A comprehensive electron wavefunction analysis toolbox for chemists, Multiwfn. *J. Chem. Phys.* **2024**, *161*, No. 082503.
(40) Falivene, L.; Cao, Z.; Petta, A.; Serra, L.; Poater, A.; Oliva, R.; Scarano, V.; Cavallo, L. Towards the online computer-aided design of catalytic pockets. *Nat. Chem.* **2019**, *11*, 872–879.
(41) Rusconi, Y.; D'Alterio, M. C.; De Rosa, C.; Coates, G. W.; Talarico, G. Disclosing multiple factors influencing enantioselective copolymerization of CO_2 with *meso*-epoxides using β-diiminate Zn catalysts. *Green Chem.* **2025**, *27*, 4196–4204.
(42) Gesslbauer, S.; Savela, R.; Chen, Y.; White, A. J. P.; Romain, C. Exploiting Noncovalent Interactions for Room-Temperature

https://doi.org/10.1021/acscatal.6c01584
ACS Catal. 2026, 16, 9397−9405

Heteroselective *rac*-Lactide Polymerization Using Aluminum Catalysts. *ACS Catal.* **2019**, *9*, 7912–7920.
(43) D'Anania, O.; Rusconi, Y.; Zunino, R.; D'Alterio, M. C.; De Rosa, C.; Talarico, G. Modulating selectivity in polymerization catalysis through noncovalent interactions: insights from experiments and DFT studies. *Coord. Chem. Rev.* **2026**, *553*, No. 217563.
(44) Falivene, L.; Cavallo, L.; Talarico, G. Buried Volume Analysis for Propene Polymerization Catalysis Promoted by Group 4 Metals: A Tool for Molecular Mass Prediction. *ACS Catal.* **2015**, *5*, 6815–6822.
(45) Hador, R.; Botta, A.; Venditto, V.; Lipstman, S.; Goldberg, I.; Kol, M. The Dual-Stereocontrol Mechanism: Heteroselective Polymerization of *rac*-Lactide and Syndioselective Polymerization of *meso*-Lactide by Chiral Aluminum Salan Catalysts. *Angew. Chem., Int. Ed.* **2019**, *58*, 14679–14685.
(46) Huang, H.-Y.; Ren, B.-H.; Xie, M.; Huang, Y.-T.; Li, K.; Cai, Z.; Lu, X.-B.; Zhu, J.-B. Access to Polyhydroxyalkanoates with Diverse Syndiotacticity via Polymerization by Spiro-Salen Complexes and Insights into the Stereocontrol Mechanism. *Angew. Chem., Int. Ed.* **2024**, *64*, No. e202419494.
(47) Ovitt, T. M.; Coates, G. W. Stereochemistry of Lactide Polymerization with Chiral Catalysts: New Opportunities for Stereocontrol Using Polymer Exchange Mechanisms. *J. Am. Chem. Soc.* **2002**, *124*, 1316–1326.
(48) Ovitt, T. M.; Coates, G. W. Stereoselective Ring-Opening Polymerization of *rac*-Lactide with a Single-Site, Racemic Aluminum Alkoxide Catalyst: Synthesis of Stereoblock Poly(lactic acid). *J. Polym. Sci. Pol. Chem.* **2000**, *38*, 4686–4692.
(49) Moccia, S.; D' Alterio, M. C.; Romano, E.; De Rosa, C.; Talarico, G. Stereoselectivity Control Interplay in Racemic Lactide Polymerization by Achiral Al-Salen Complexes. *Macromol. Rapid Commun.* **2025**, *46*, No. 2400733.
(50) Peterson, A.; Hador, R.; Pink, M.; Popowski, Y.; Kol, M.; Tolman, W. B. Defining Stereochemistry in the Polymerization of Lactide by Aluminum Catalysts: Insights into the Dual-Stereocontrol Mechanism. *J. Am. Chem. Soc.* **2022**, *144*, 20047–20055.
(51) Press, K.; Goldberg, I.; Kol, M. Mechanistic Insight into the Stereochemical Control of Lactide Polymerization by Salan-Aluminum Catalysts. *Angew. Chem., Int. Ed.* **2015**, *54*, 14858.
(52) Han, J. W.; Hollmann, F.; Luque, R.; Song, I. K.; Talarico, G.; Tatsumi, T.; Yan, N. Molecular Catalysis for the Chemistry of the future: a perspective. *Mol. Catal.* **2022**, *522*, No. 112233.

https://doi.org/10.1021/acscatal.6c01584
ACS Catal. 2026, 16, 9397−9405